PCCP

Accepted Manuscript

This is an *Accepted Manuscript*, which has been through the Royal Society of Chemistry peer review process and has been accepted for publication.

Accepted Manuscripts are published online shortly after acceptance, before technical editing, formatting and proof reading. Using this free service, authors can make their results available to the community, in citable form, before we publish the edited article. We will replace this *Accepted Manuscript* with the edited and formatted *Advance Article* as soon as it is available.

You can find more information about *Accepted Manuscripts* in the Information for Authors.

Please note that technical editing may introduce minor changes to the text and/or graphics, which may alter content. The journal's standard Terms & Conditions and the Ethical guidelines still apply. In no event shall the Royal Society of Chemistry be held responsible for any errors or omissions in this *Accepted Manuscript* or any consequences arising from the use of any information it contains.

ROYAL SOCIETY OF CHEMISTRY

www.rsc.org/pccp

Fabrication of Hierarchical ZnO/CdS Heterostructured Nanocomposites for Enhanced Hydrogen Evolution from Solar Water Splitting

Soumita Mukhopadhyay[a,c], Indranil Mondal[b,c], Ujjwal Pal*[b] and Parukuttyamma Sujatha Devi*[a]

Physical Chemistry Chemical Physics Accepted Manuscript

[a]*Nano-Structured Materials Division, CSIR-Central Glass and Ceramic Research Institute, Kolkata 700032, India.*

[b]*Chemistry and Biomimetics Group, CSIR-Central Mechanical Engineering Research Institute, M.G Avenue, Durgapur-713209, West Bengal, India.*

[a,b]*India Network Institute of Solar Energy, (CSIR-NISE) and Academy of Scientific and Innovative Research (AcSIR), New Delhi , India*

[c] *These two authors contributed equally.*

**psujathadevi@cgcri.res.in;psujathadevi@gmail.com, upal03@gmail.com*

§ Electronic supplementary information available:

FESEM image and TEM of native ZnO rods and particles, and amount of the hydrogen evolved on varying the concentration of sacrificial agent in the heterostructured nanocomposite at optimized condition.

Abstract

ZnO/CdS heterostructured nanocomposites were fabricated by sequential sonochemical and hydrothermal methods from ZnO rods and particles with enhanced light harvesting capability and photostability. Interestingly, in the composite of CdS sensitized ZnO rods, both ZnO and CdS exist in the hexagonal wurtzite form having different morphologies. On the other hand, in the composite of CdS sensitized ZnO particles, ZnO exists in the hexagonal wurtzite form whereas CdS in the cubic form but with a similar morphology. The synthesized photocatalysts under simulated solar irradiation of exhibited hydrogen evolution rates of 870 and 1007 $\mu molh^{-1}g^{-1}$ for ZnO rod/CdS and ZnO nanoparticle/CdS composites, respectively, compared to the native ZnO (40 $\mu molh^{-1}g^{-1}$ for rods and 154 $\mu molh^{-1}g^{-1}$ for particles) and CdS (208 $\mu molh^{-1}g^{-1}$) structures. The apparent quantum yield of CdS was only 1.2%, whereas the composites exhibited much higher quantum yields of 4.9 and 5.7%, respectively. Our results confirmed that morphology of the host matrix ZnO played a crucial role in forming ZnO/CdS heterostructures with improved interface for direct Z-scheme mechanism with enhanced hydrogen evolution efficiency.

Physical Chemistry Chemical Physics Accepted Manuscript

Introduction

Recently, intense studies have been performed on designing new semiconducting photocatalysts for hydrogen production through solar water splitting by harvesting maximum light, a process commonly known as artificial photosynthesis.[1-4] Most of the known photocatalysts for this two electron hydrogen evolution reaction are either wide band gap semiconductors such as TiO_2, ZnO, SnO_2 etc which can harvest photons only in the UV region covering only ~ 4% of the entire solar spectrum or narrow band gap semiconductors such as chalcogenides to generate electron-hole pairs.[1-4] Photocorrosion and the rapid recombination of photo excitons inevitably interrupt the outward dispersion of photocarriers and consequently decrease the photocatalytic hydrogen evolution efficiency of most of such materials. Therefore, diverse methodologies such as doping with transition metals/nonmetals, surface modification via noble metal deposition or coupled heterojunction formation have been adopted to expand their spectral response towards visible light as well as to minimize the recombination of photocarriers and enhance the photostability.[5-8] Generally, single phase photocatalysts exhibit less efficiency possessing low separation efficiency of photocarriers as compared to the integrated multi-semiconductor systems. Nanoscale hybrids possessing significant compensation in promoting the separation of excitons which maintain the reduction and oxidation reactions at two different counter parts are also being investigated. It is an accepted fact that no single semiconducting materials can meet the suitable band gap of 1.8 -2.4 eV, matching energy band for H_2 evolution, high quantum efficiency and stability for photocatalytic water splitting. Thus, in order to photosensitize wide band gap semiconducting oxides towards visible region, integrated coupling with narrow band semiconductors such as In_2O_3, Fe_2O_3, CuO, CuS, CdS, ZnS and ZnSe which possess different redox energy levels provide an attraction to achieve more efficient charge

Physical Chemistry Chemical Physics Accepted Manuscript

separation prolonging the lifetime of the charge carriers.[9-24] In this regard, ZnO coupled with CdS is considered to be a potential candidate for hydrogen evolution due to their compatible lattice structure which leads to strong interaction, consequently facilitating the effective interband charge transfer from CdS to ZnO. In addition, their more negative conduction band edge than the H_2/H^+ redox potential is more suitable for H_2 evolution.[10-14,18-21] In recent times, different types of nanostructured ZnO/CdS composites have been successfully employed for the photocatalytic hydrogen evolution studies.[25-32] Among those, the most important result was reported by Wang et al., where a high hydrogen evolution efficiency of 1805 μmol h^{-1} g^{-1} was for $(ZnO)_1/(CdS)_{0.2}$ heterostructure.[25a] Surprisingly, ZnO disk/CdS and ZnO rod/CdS exhibited much lower efficiencies of 88.6 and 31.2 μmol h^{-1}, respectively.[26a] 1D nanocomposites and porous heterostructures on the other hand exhibited 155.5 μmolh^{-1} and 851 μmol $h^{-1}g^{-1}$, respectively.[31a, 13]

In this work, we explored the effect of hydrothermal deposition of CdS nanoparticles on sonochemically prepared ZnO nanostructures and their application in photocatalytic hydrogen evolution under simulated light irradiation. Two different structures of ZnO, viz. ZnO-hexagonal rods and mesoporous ZnO nanoparticles were coupled with CdS nanoparticles for carrying out the water splitting experiments.

Experimental

Sonochemical synthesis of ZnO rods and mesoporous particles

We have been working on various morphologies of ZnO for dye sensitized solar cells.[32,33] The detailed synthesis procedure of ZnO rods has been reported in our previous work[33] where zinc acetate dihydrate [$Zn(OAc)_2$. $2H_2O$] was used as the zinc precursor. Mesoporous ZnO nanoparticles (NPs) were also prepared by the sonochemical process (ultrasonic processor of power 250 W, ultrasonic frequency 30 kHz (SS4 probe diameter, 25 mm) using 250 mL 0.05

Physical Chemistry Chemical Physics Accepted Manuscript

(M) aqueous solution of Zinc nitrate hexahydrate ($Zn(NO_3)_2.6H_2O$, 99.9%, Merck Ltd. India) as zinc source and triethanolamine (TEA) as a structure directing agent maintaining a molar concentration of TEA to Zn^{2+} as (1:1). In both the cases ammonium hydroxide [30% GR, Merck Ltd. Mumbai, India] was used as a precipitating agent and the solution pH was maintained at 9±0.5. The as-prepared product was centrifuged at ~11,000 rpm and washed with distilled water and ethanol for several times to remove TEA followed by drying under the IR lamp. The as-obtained product was heat-treated at 450 ^oC for 4 h to remove the residual template.

Hydrothermal Synthesis of ZnO/CdS heterostructured nanocomposite

ZnO/CdS heterostructures were prepared by a hydrothermal method. Initially, 100 mg each of ZnO rods and nanoparticles were suspended separately in 20 ml of HPLC grade water and required amount of $Cd(NO_3)_2.4H_2O$ was added into the resulting aqueous suspension. The pH of the mixed solution was maintained at 8 by the addition of 0.05 M $NH_3{\cdot}H_2O$ solution. The resulting solution was stirred for 30 min followed by the addition of required amount of thiourea where x mM is the amount of $Cd(NO_3)_2$. $4H_2O$ present in the solution. High purity (99.99%) argon gas was bubbled through the mixture for 30 min to expel dissolved oxygen, followed by stirring for 1h. To this mixed solution, 5 ml of mercaptoethanol was added and the final mixture was transferred to a 50 ml Teflon lined autoclave and maintained the autoclave at 150 °C for 24 h. After cooling at room temperature the yellowish precipitate was retrieved by centrifugation at 4000 rpm and washed with DI water and ethanol several times and subsequently dried at 70 °C for overnight in air. The final products were designated as ZC-1 and ZC-2 for rod and nanoparticle composites, respectively.

Physical Chemistry Chemical Physics Accepted Manuscript

Physico chemical characterization

The products' phase purity was characterized by X-ray diffraction measurements on a X'pert pro MPD XRD of PANalytical system with CuKα radiation (λ=1.5406 A˚). The particle morphology and high-resolution transmission electron microscopy (HRTEM) were investigated by transmission electron microscopy (TEM) on a Tecnai G2 30ST (FEG) Ultra High Resolution Transmission Electron Microscope operating at 200 kV. Solid powder surface morphology was studied using energy dispersive X-ray (EDX) study and corresponding elemental mapping images were taken by field emission scanning electron microscopy on Supra 35VP (Carl Zeiss) Field Emission Scanning Electron Microscope (FESEM) operating at 20 kV. The diffuse reflectance spectra were recorded on a UV-Vis-NIR Spectrophotometer (SHIMADZU UV-3600). The emission characteristics were recorded at room temperature on a Steady State Spectrofluorometer (QM-40, Photon Technology International, PTI) using a 150 watt Xenon lamp as an excitation source, at excitation wavelengths of 390 nm and 345 nm using a band pass of 5 nm. X-ray photoemission spectroscopy measurements were carried out in a PHI 5000 Versa probe II scanning XPS microprobe (ULVAC-PHI, U.S.). The measurements were performed at room temperature and at a base pressure better than 6×10^{-10} mbar. All spectra were recorded with monochromatic Al Kα (hν = 1486.6 eV) radiations with a total resolution of about 0.7 eV and a beam size of 100 μm.

Photocatalytic performance studies

The photocatalytic H_2 generation experiments were carried out in a 100 mL Pyrex glass reactor with flat optical entry window and external cooling jacket. 20 mL of the aqueous suspension containing 20 mg photocatalyst and sacrificial electron donor (SED) was the reaction mixture. The reactor was sealed with rubber septum and sonicated to suspend the

Physical Chemistry Chemical Physics Accepted Manuscript

catalyst completely in the water/SED system. Thereafter, the photoreactor was deaerated by bubbling argon for 30 min to remove the dissolved air before light irradiation. The reaction mixture was further stirred and irradiated by a Newport Xenon lamp (Newport, USA, model no: 66924) working at 400 W with an average intensity ~ 2 Sun (0.195 W/cm^2). Intensity of the light has been measured using optical power/energy meter, Newport, model: 842-PE. The distance between the lamp and the photoreactor was fixed at 8 inches. The gaseous products produced were analyzed by Chemito 1000 GC equipped with 5A molecular sieve column, a thermal conductivity detector and Argon as the carrier gas.

Results and discussion

Structural, chemical and morphological study

In Fig.1, the XRD patterns of the as-formed ZC-1 and ZC-2 nanocomposites are presented along with that of the standard JCPDS data of cubic-CdS(C), hexagonal-CdS(H) and

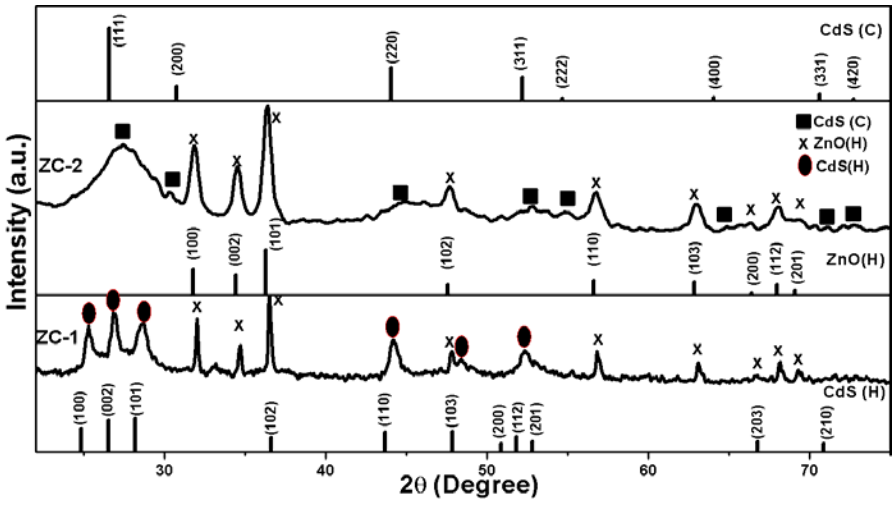

Fig. 1 The XRD patterns of ZC-1 and ZC-2 along with JCPDS files of CdS and ZnO are also shown in the figure for comparison.

Physical Chemistry Chemical Physics Accepted Manuscript

hexagonal-ZnO(H). It could be confirmed from the XRD patterns that in ZC-1, a mixture of hexagonal ZnO and hexagonal CdS exist, whereas, in ZC-2 sample ZnO exists in the hexagonal wurtzite form and CdS in the cubic zinc blend form. All the diffraction peaks of cubic CdS appeared in ZC-2, as indicated in the XRD pattern. The broad reflections confirm the nanocrystalline nature of the formed CdS particles. No other diffraction reflections corresponding to CdO or ZnS were presented in the XRD pattern confirming the phase purity of the heterostructured nanocomposites.

In Fig. 2, the TEM images of ZC-1 and ZC-2 nanocomposites with their corresponding HRTEM images are presented. The morphology of the starting ZnO rods and particles are presented in Fig. S1. Fig. 2 (a) reveals the rough surface of ZnO/CdS nanocomposite,

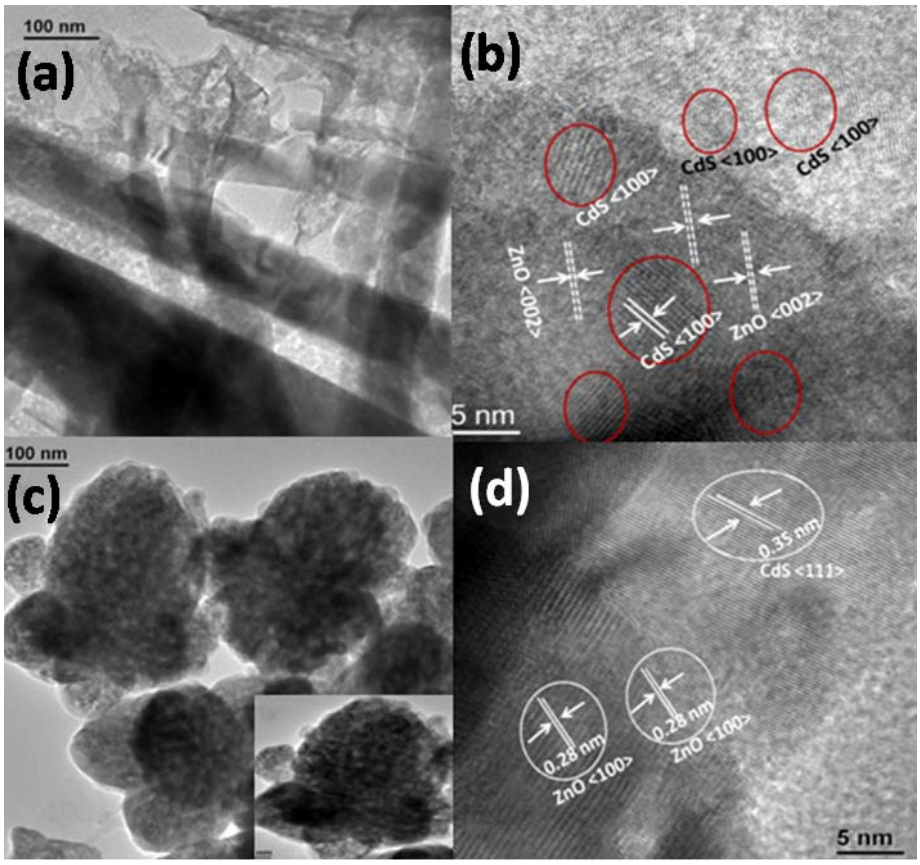

Fig. 2 a & c represent the TEM images of ZC-1 and ZC-2 composites respectively and b & d corresponds to the respective HRTEM images of ZC-1 and ZC-2.

Physical Chemistry Chemical Physics Accepted Manuscript

composed of spatially interconnected quasi-spherical tiny CdS nanoparticles occupying the exterior portion of ZnO nanorods thereby revealing the formation of a heterostructure of ZnO rods and CdS particles. The HRTEM image shown in Fig. 2b indicates the well-resolved two dimensional lattice fringes with a spacing of 0.26 nm corresponding to the (002) plane of ZnO on which CdS (100) crystal planes with a lattice fringe of 0.35 nm are formed. Fig. 2(c) depicts the formation of a porous flower like morphology by the assimilation of self assembled ZnO/CdS nanoparticles. The HRTEM image shown in Fig. 2d clearly indicates well-resolved intersected two dimensional lattice fringes with a spacing of 0.33 nm and 0.28 nm corresponding to the CdS (111) and ZnO (100) crystal planes, respectively. In both cases, the ZnO/CdS interface was highly crystalline which confirms the phase purity of the heterostructured nanocomposites, which was also supported by the XRD pattern shown in Fig. 1. Interestingly, independent existence of ZnO and/or CdS nanoparticles could be observed from the solid powder surface morphology and corresponding elemental mapping carried out by the FESEM study. In Fig. 3 the surface morphology and corresponding elemental mapping of ZC-1 and ZC-2 nanocomposites are presented.

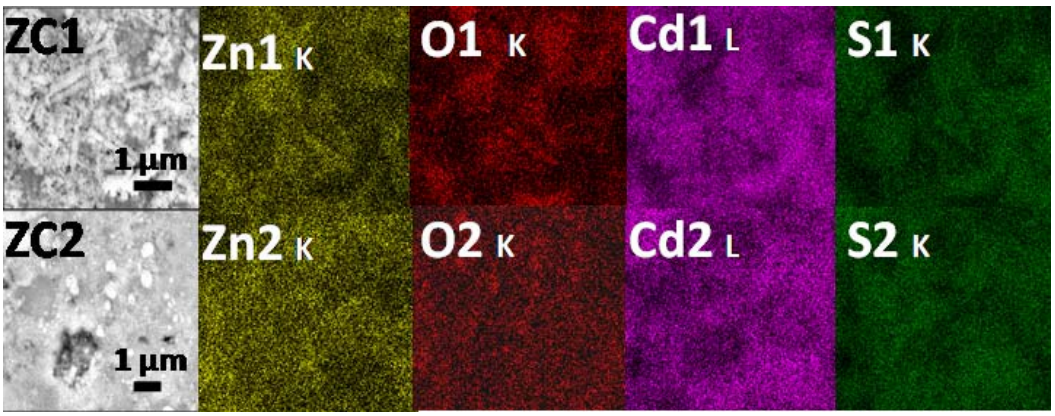

Fig. 3 FESEM surface morphology and corresponding elemental mapping of ZC-1 and ZC-2 nanocomposite recorded on powder samples.

Physical Chemistry Chemical Physics Accepted Manuscript

The elemental mapping presented in Fig. 3, provided a strong evidence for the coexistence of uniformly distributed ZnO (NPs and/or rods) and CdS NPs within the nanocomposites and easily ruled out the presence of CdO or ZnS as impurity in our samples. The formation of an intimately mixed composite of ZnO/CdS is in agreement with the suggestion of Fang et al. that due to the similar chemical properties of oxygen and sulfur there is a strong affinity of *in situ* generated sulfide ions to be captured by the oxygen vacancies located in the ZnO surface ultimately leading to the intimate growth of CdS nanoparticles with ZnO.[11]

In Fig. 4a, the UV-Vis diffuse reflectance spectra of ZC-1 and ZC-2 composites and their corresponding native ZnO are shown. The native ZnO exhibited an absorption edge at 374 ±2 nm, with no apparent absorption in the visible region, whereas ZnO/CdS composites display two spatially distinguishable absorption band-edges in the range of 430–540 nm and in the ultraviolet region thereby confirming the successful incorporation of CdS nanoparticles in the composite. In addition, the occurrence of a sharp dip in the absorbance spectra authenticates the presence of separate phases of ZnO and CdS, thus confirms our argument for the formation of a heterostructured nanocomposite. Moreover, the absorption edge of the composite has been extended to the visible up to 540 nm due to the incorporation of CdS on ZnO which could help to harvest the UV as well as visible component of the solar radiation.[12] CdS nanoparticles deposited on ZnO rods and porous ZnO nanoparticles exhibited different band gaps of 2.52 eV and 2.6 eV corresponding to hexagonal and cubic phases of CdS again confirming the formation of two different crystallographic phases of CdS depending on the morphology of ZnO host.[34] In addition to the absorption studies, the emission characteristics of the composites were also investigated at room temperature at different excitation wavelengths of 345 nm and 390 nm to investigate emission characteristics of the host materials ZnO and CdS, respectively. In Fig. 4(b & c), the emission spectra of ZC-1 and ZC-2 samples (excited at 345 nm) along with the emission spectra of native ZnO and absorption

Physical Chemistry Chemical Physics Accepted Manuscript

spectrum of CdS nanoparticles are presented. Fig. 4d shows, the emission spectra of ZC-1 and ZC-2 samples (excited at 390 nm) along with the emission spectrum of native CdS nanoparticles.

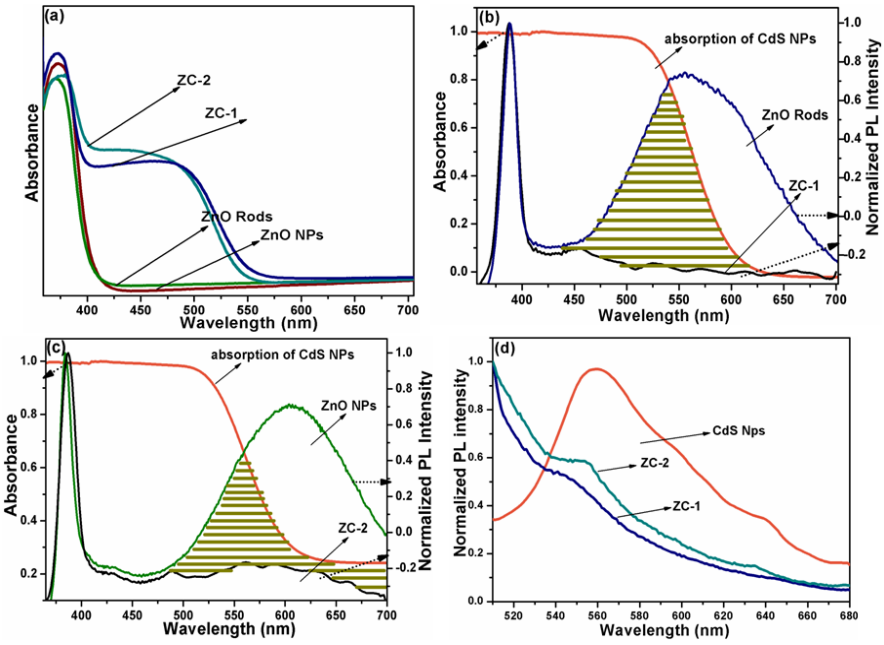

Fig. 4 (a) Absorption spectra of solid ZnO rods, particles, ZC-1 and ZC-2, (b & c) emission spectra of ZC-1 and ZC-2 excited at 345 nm wavelength compared with the emission of native ZnO, which is overlapped with the absorption spectrum of CdS NPs and (d) emission spectra of ZC-1, ZC-2 and native CdS NPs excited at 390 nm wavelength. All the spectra were taken at room temperature.

Native ZnO exhibited two distinct peaks; a sharp peak at 383 ±1 nm and a broad peak in the 400-700 nm regions. The broad band in the 450–700 nm regions in the emission spectrum corresponds to the defect related visible emission exhibited by ZnO. The Gaussian curve fitted defect emission of native ZnO samples are presented in Fig. S2. Deconvolution of the respective spectra (shown in Fig. S2), reflects that the broad visible emission of native ZnO is an overlapping of two emission bands at 560 ±2 nm and 620 ±2 nm attributed to doubly

Physical Chemistry Chemical Physics Accepted Manuscript

ionized oxygen vacancy ($V_o^{\cdot\cdot}$) and chemisorbed/interstitial oxygen (Oi), respectively.[33] In both cases, (ZC-1 and ZC-2) the broad band between 450–700 nm in the emission spectrum corresponding to the defect related green–yellow emission, is suppressed drastically compared to the band edge emission NBE (383 ±1 nm) on loading with CdS. As the emission of native ZnO overlapped with the absorption of CdS NPs, the electron–hole recombination of ZnO nanostructures may be attenuated by CdS nanoparticles by the fluorescence resonance energy transfer (FRET) mechanism, where the photoexcited electrons in the ZnO conduction band (CB) could transfer to the valence band (VB) of CdS resulting in quenching of the fluorescence of ZnO.[28] The absorption-emission interaction as well as the quenching of defect related visible emission was relatively less in case of ZC-2 as compared to ZC-1. However, in both cases a strong indication of fluorescence quenching was observed. CdS possessing narrower energy band-gap helps in the effective separation of photocarriers reducing their recombination and also modifies the surface properties of native ZnO nanostructures.[10-12,20-22,24,27] Interestingly in Fig. 4d, also a similar observation has been noticed. The native CdS nano particle on excitation at 390 nm exhibited a strong visible emission at 555 ±3 nm, whereas ZnO/CdS nanocomposites (ZC-1 and ZC-2) displayed feeble emission bands which were blue shifted slightly. The fluorescence studies on the composite samples thus confirmed that ZnO/CdS nanocomposites (ZC-1 and ZC-2) exhibited weaker emission as compared to native ZnO or CdS, suggesting the effective transfer of charge carriers-photoexcited electrons and holes between ZnO and CdS resulting in reduced recombination probability in the composite. The charge carriers with prolonged lifetime in ZnO/CdS heterostructure are beneficial for the improved photocatalytic activity and photostability.[25,30]

The chemical nature of ZnO/CdS heterostructure was also examined by XPS analysis, shown in Fig. 5. All binding energies were calibrated using the contaminant carbon (C 1s =

Physical Chemistry Chemical Physics Accepted Manuscript

283.3 eV) as the reference. From the XPS spectra, it is evident that the sample ZC-2 is composed of Zn, O, Cd and S. The position of Zn $2p_{1/2}$ and $2p_{3/2}$ binding energies occurred at 1019.7 eV and 1042.7 eV, with a spin orbit separation of 23 eV, confirm that Zn exists in the form of Zn^{2+} chemical state in the sample. The O 1s core level spectra show strong shoulders/asymmetries at the higher binding energy side (Fig. 5b) and on deconvolution, this resulted in three different components at binding energies of 528.4 eV, 530.4 eV and 531.4 eV which are closely associated with the lattice oxygen (O_L) of ZnO, surface oxygen vacancy (Ov) and chemisorbed oxygen (Oc) respectively.[10] Fig. 5c shows the narrow range scan of Cd 3*d* core level where two peaks corresponding to the binding energies of Cd $3d_{5/2}$ at 403.2 eV and the Cd $3d_{3/2}$ at 409.9 eV, respectively, are present.

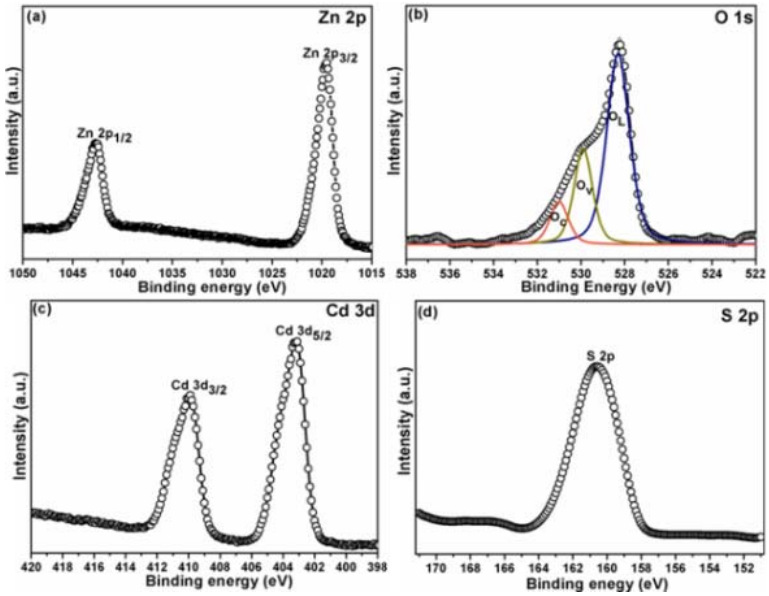

Fig. 5 XPS spectra of (a) Zn 2p, (b) O 1s (coloured line shows simulated curves), (c) Cd 3d, and (d) S 2p of ZC-2

The spin orbit splitting energy of 6.7eV is characteristics of Cd^{2+} in CdS. The position of the S 2p peak (Fig. 4d) is at about 160.6eV, which confirms that S element exists mainly in the form of S^{2-} chemical state on the sample surface.[10]

Physical Chemistry Chemical Physics Accepted Manuscript

H_2 evolution over ZnO/CdS heterostructured nanocomposites

CdS is one of the most studied visible photocatalyst for hydrogen evolution due to its narrow band gap and its ability to harvest visible light. ZnO, on the other hand is a visible inactive semiconducting oxide. A spatially and uniformly dispersed composite of ZnO/CdS synthesized here is expected to enhance the photocatalytic activity of the native materials substantially. Therefore, the photocatalytic activity of the synthesized ZnO/CdS heterostructured nanocomposites was monitored by measuring the H_2 evolution from an aqueous solution containing Na_2S/Na_2SO_3. Na_2S/Na_2SO_3 was suppose to act as a hole scavengers for the photocatalyst. We also compared the catalytic activity of the native ZnO and CdS nanoparticles for comparison. The control experiments without any photocatalyst confirmed no H_2 evolution in presence of light. Native ZnO rods and ZnO NPs exhibited hydrogen evolution efficiencies of ~ 40 $\mu molh^{-1}g^{-1}$ and 154 $\mu molh^{-1}g^{-1}$, respectively, under simulated light irradiation. Similarly, CdS prepared under identical conditions exhibited a H_2 evolution rate of only 208 $\mu molh^{-1}g^{-1}$. Interestingly, when the heterostructured nanocomposite of ZnO rods and nanoparticles were coupled with CdS nanoparticles, hydrogen evolution efficiency was drastically enhanced to 870 $\mu molh^{-1}g^{-1}$ with an apparent quantum yield (AQY) of ~ 5 for ZC-1 and 1007 $\mu mol\ h^{-1}\ g^{-1}$ with AQY of ~ 5.7 for ZC-2, respectively, under similar experimental conditions. The porous morphology has allowed the photogenerated carriers to be collected over a relatively short distance resulting in a high AQY for the collection of photogenerated carriers.

Fig. 6 (a, b) depict the amount of the hydrogen evolved on varying the photocatalysts and ZnO:CdS ratio, respectively. The lowest rate of H_2 evolution was from native ZnO nanoparticle and the highest from ZnO/CdS nanoparticle composite (Fig. 6b). It is evident that in both cases, the composites exhibited enhanced H_2 evolution rate compared to the host matrices, ZnO and CdS. The hydrogen evolution gradually increases with increase in the

Physical Chemistry Chemical Physics Accepted Manuscript

concentration of CdS with a maxima exhibited by a 1:1 ratio of ZnO:CdS (Fig. 6b). In Fig. 6c & d) the hydrogen evolution rate and the corresponding Apparent Quantum Yield (AQY) keeping the molar ratio of ZnO:CdS as 1:1 is presented. In both the cases, ZnO rods/NPs coupled with CdS NPs at a molar ratio of 1:1 exhibited the highest hydrogen evolution rate, which gradually decreased with increase in the CdS molar ratios. The effect of the concentration of the sacrificial electron donating (SED) agent was studied over the range of 0.025 M to 0.4 M as shown in Fig. S3. Only marginal difference was found in the H_2 production for 0.1 and 0.4 M aqueous SED solution as shown in Fig. S3. So, 0.1 M SED

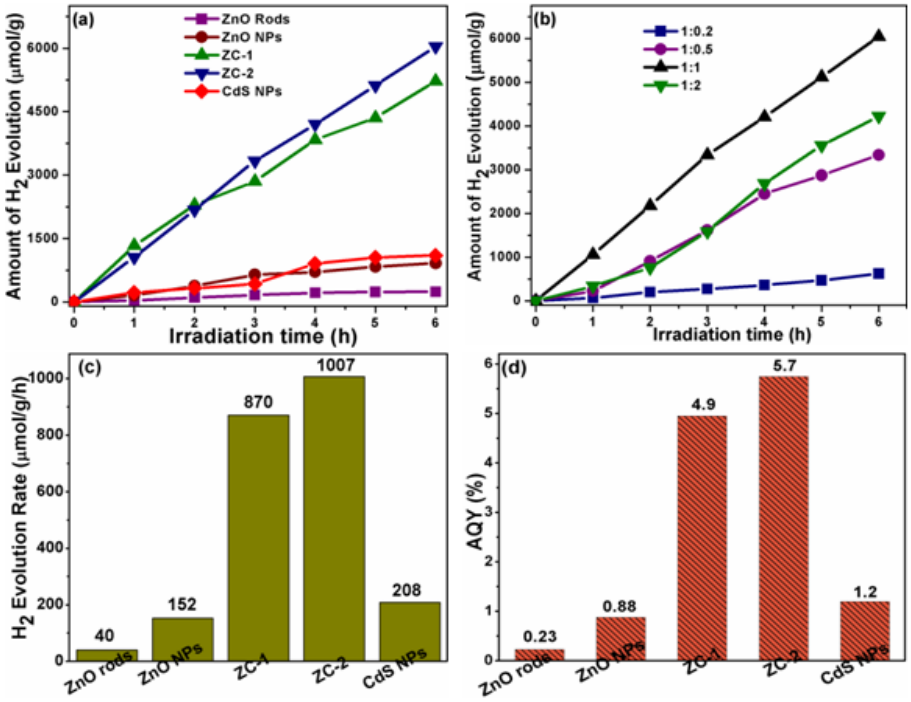

Fig. 6 Amount of the hydrogen evolved on (a) various photocatalysts, (b) ZnO NPs:CdS at different ratios (c) hydrogen evolution rate of various structures and (d) corresponding Apparent Quantum Yield (AQY) at optimized condition.

concentration was optimized to carry out further experiments. The AQY of CdS was only 1.2%, whereas ZC-1 and ZC-2 exhibited much higher AQY of 4.9 and 5.7, respectively. The enhanced hydrogen evolution rate in both heterostructured nanocomposites as compared to

Physical Chemistry Chemical Physics Accepted Manuscript

their native host ZnO may be governed by the enhanced absorption-emission interaction (shown in Fig. 4b & c) in the visible region resulting in increased light harvesting under simulated solar irradiation. The result exhibited by the ZnO/CdS particles in our case is much higher than the recent report by Zou et al., for 1D-CdS/ZnO which was only 851 $\mu molh^{-1}g^{-1}$ [13].

This could be due to the enhanced photosensitization, resulting from the photocarrier transport along the one dimentional structure of ZnO rods and the large exposed active surface sites[24] of meso-porous ZnO particles, respectively. In order to evaluate the photostability of ZC-1 and ZC-2 photocatalysts for practical application, consecutive seven runs were carried out with evacuation after each run and SED was refreshed after consecutive five runs as shown in Fig. 7. Both composites showed similar trend over prolonged irradiation. Hydrogen evolution efficiency diminished after 2nd run and leveled off in the next three consecutive runs. The decreasing activity was observed due to the consumption of the sacrificial agent.

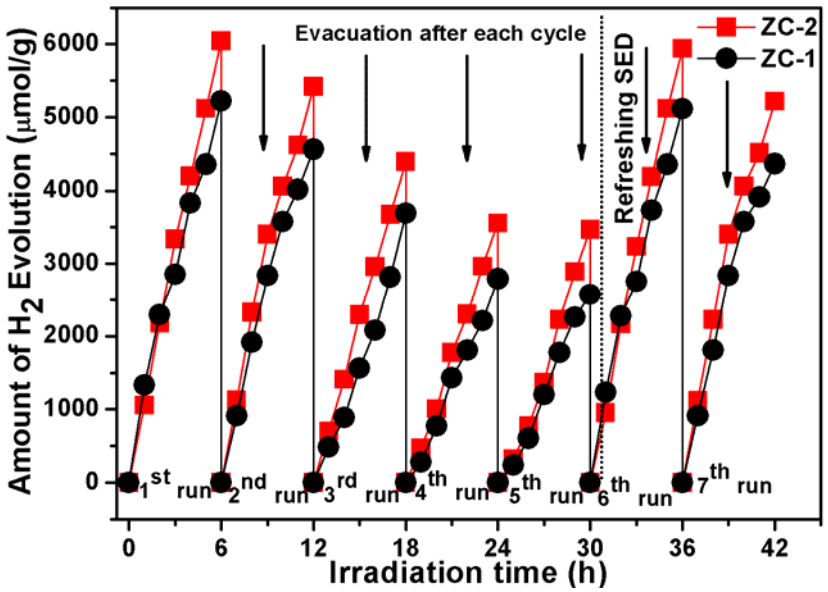

Fig. 7 Reproducibility study of photocatalytic hydrogen evolution under optimized condition

Refreshing the sacrificial electron donating solution (SED) after fifth runs, the photocatalytic activities were again recoiled to the initial stage indicating the excellent stability of these

Physical Chemistry Chemical Physics Accepted Manuscript

nanocomposites for photocatalytic hydrogen evolution. The stability of cadmium chalcogenide QD's is still very poor owing to the hole-induced photocorrosion. But in this case, the composites under simulated solar irradiation (~2 Sun), could harvest more photons and generate more electron-hole pairs followed by recombination of conduction band electrons in one component to the holes present in other component in presence of sacrificial electron donor (SED), which mutually compensate the photocorrosive nature to sustain photostability compared to their native components.[29]

The photocatalytic activity in ZnO/CdS may occur via two plausible pathways as reported by many investigators - (i) One common mechanism could be the flow of photoexcited electrons from the conduction band electrons of CdS to the conduction band of ZnO, and the flow of holes in the reverse direction resulting in the reduction of H_2O to H_2 gas.[24] (ii) In another path, the photoexcited conduction band electrons from ZnO recombines with the valence band holes of CdS and the residual electrons on CdS and holes on ZnO will induce the redox reactions for H_2 evolution which is known as the Z-scheme.[3,13,25] In presence of sacrificial electron donor, the photogenerated holes (h^+) in the ZnO could quickly transfer to solvated S^{2-} and SO_3^{2-} to produce S_2^{2-} and SO_4^{2-}, respectively, as shown in equation (1-3). According to the direct Z scheme mechanism suggested by others, the following are the most probable reactions.[13, 25]

$$2\ e^-_{CdS} + 2\ H_2O \longrightarrow H_2 + 2\ OH^- \quad \text{..... (1)}$$

$$2\ h^+_{(ZnO)} + SO_3^{2-} + 2\ OH^- \longrightarrow SO_4^{2-} + H_2O \quad \text{..... (2)}$$

$$2\ S^{2-} + 2\ h^+_{(ZnO)} \longrightarrow S_2^{2-} \quad \text{..... (3)}$$

Both ZC-1 and ZC-2 exhibited quenching of the PL intensity which suggests reduced recombination of charge carriers. The minimum rate of recombination is expected to significantly enhance the photocatalytic activity. We believe that the Z scheme mechanism is facilitated in the studied systems under simulated solar irradiation (~ 2 Sun) due to the reduced recombination rate as has been confirmed through PL quenching studies.[25, 30]

Physical Chemistry Chemical Physics Accepted Manuscript

The conduction band position (E_{cb}) of CdS nanoparticles calculated using the equation[35] E_{cb} = X- E_c -0.5E_g, (where E_c represents the energy of free electrons on the hydrogen scale (4.5 eV), X is the electronegativity of the semiconductor, and E_g represents the bandgap of the semiconductor) shows -0.585 eV and -0.62 eV (*vs.*NHE), respectively for ZC-1 and ZC-2 heterostructured nanocomposites. As photogenerated electrons are more negative in ZC-2 nanocomposite, this could further facilitate in H_2 production compared to ZC-1.

If conventional charge separation occurs in the heterojunction composite, then conduction band electrons from CdS will migrate to the conduction band of ZnO and holes (h^+) in the valence band of ZnO will migrate to the valence band of CdS. Then the probability of H_2 evolution will be less in the composite as compared to the native CdS, as conduction band edge potential as well as reducing capability of electrons in $(CB)_{ZnO}$ is less as compared to than that of CdS. Similarly, oxidation potential of holes in $(VB)_{CdS}$ will be very less as compared to ZnO which will diminish the photostability of the heterojunction composite. As a result composite will show detrimental activity as compared to the host materials.

As the CB of CdS is more negative than ZnO and hence energy transfer may also happen from CdS to ZnO, where CdS purely act as sensitizer as reported by Zou et. al.[13] However, in our study, CdS is likely to take part in direct Z-Scheme path where upon irradiation, where electron from ZnO's CB combine with the hole in CdS VB. This fact is well supported by the PL spectroscopy which is an important tool to investigate the efficiency of trapping, separation, and transfer of charge carriers in semiconductors. PL spectra displayed lower PL intensity of ZnO@CdS (ZC-1 and ZC-2) composite in comparison to bare CdS. It is established that the charge-carrier transfer between different parts of composites usually results in the weakening of PL emission bands. [30] In our case, the direct Z-scheme interface charge-carrier transfer should be responsible for the weakened PL emission bands of the CdS/ ZnO. It is worth mentioning that the intimate contact between ZnO NPs and CdS NPs in ZC-2 achieved through the porous network of ZnO, helps in an improved synergistic effect in enhancing the photocatalytic activity of ZnO particles/CdS particles resulting in a hydrogen evolution rate of 1007 $\mu molh^{-1}g^{-1}$ which is many times higher compared to the native systems. In Table 1, we have compared the latest results of ZnO/CdS composites employed for the photocatalytic hydrogen evolution studies. It is convincing that the performance of CdS nanoparticles-decorated mesoporous ZnO nanoparticles are excellent candidates for solar water splitting with enhanced photocatalytic activity.

Physical Chemistry Chemical Physics Accepted Manuscript

Table 1: Comparative results of photocatalytic hydrogen evolution based on earlier reports using similar systems in the literature.* Rate has been reported using 0.1g photocatalyst.

Photocatalyst	**Amount of Photocatalyst (mg)**	**Irradiation source details**	**Rate of H_2 production (μmol/g/h)**	**Reference**
1D porous CdS/ZnO	10	500 W Xe lamp equipped with a glass optical filter (λ > 400 nm).	851	[13]
ZnO/CdS	200	300 W Xe lamp	1805	[25a]
ZnO disk/CdS	100	300 W Xe lamp.	88.6*	[26]
ZnO rod/CdS			31.2*	
1D CdS/ZnO core/shell nanofibers	50	500W Xe lamp equipped with a glass optical filter (λ > 420 nm).Intensity: 181 mW cm^{-2}	354	[29]
1D CdS/ZnO core/shell nanorod	200	300 W Xe lamp equipped with a glass optical filter (λ > 400 nm).Intensity: 135 m W/cm^2	2960	[25b]
ZnO/CdS nanourchin	100	500 W tungsten halogen lamp. equipped with a UV cut off filter	1008*	[26b]
1D CdS/ZnO and 1 wt% Pt as co-catalyst.	100	400 W mercury vapour lamp.	155.5*	[31a]
ZnO/ZnS/CdS	10	300 W Xe lamp equipped with a glass optical filter (λ > 400 nm).Intensity: 0.6 W/cm^2	1725	[31b]
ZnO rod/CdS (ZC-1)	20	400 W Xe lamp. Intensity: 0.195 W/cm^2 (~ 2 Sun)	870	Present work
ZnO NPs/CdS(ZC-2)			1007	

Physical Chemistry Chemical Physics Accepted Manuscript

Conclusions

Well dispersed ZnO/CdS heterostructured nanocomposites were successfully prepared by following a sequential sonochemical and hydrothermal methods of synthesis. The XRD and TEM together with confirmed the formation of hexagonal ZnO rods and hexagonal CdS particles in one case (ZC-1) and hexagonal ZnO particles and cubic CdS particles (ZC-2) in another case. Because of the coupling effects of the two semiconductors, the visible-light absorption ability of these nanostructured heterocomposites was enhanced and as a result they displayed ~ 6.6 to 22 times higher photocatalytic activity compared to the corresponding ZnO for light induced water splitting. The sensitization efficiently extends the absorption edge up to 540 nm and reduces the electron–hole recombination of ZnO nanostructures probably via fluorescence resonance energy transfer (FRET) mechanism resulting in 22 times higher HER as compared to the native ZnO rods. In addition, the porous lotus like structured ZC-2 with cubic CdS exhibited the highest HER of 1007 μmol h^{-1} g^{-1} owing to its uniformly structured porous nature with more active surface sites. In conclusion, we have successfully demonstrated the excellent performance of CdS nanoparticles-decorated ZnO rods and mesoporous ZnO nanoparticles for solar water splitting with enhanced photocatalytic activity, reproducibility, stability and above all compromise over the usage of corrosive CdS.

Acknowledgements

SM is indebted to the University Grant Commission (UGC) Govt. of India for the award of Senior Research Fellowship. IM acknowledges AcSIR for Ph.D enrolment. PSD acknowledges MNRE for financial support under CSIR-TAPSUN programme and UP acknowledges CSIR for financial support under TAPSUN.

Physical Chemistry Chemical Physics Accepted Manuscript

Notes and References

1 F. E. Osterloh, *Chem. Mater.*, 2008, **20**, 35–54.

2 X. Chen, S. Chen, L. Guo, and S. S. Mao, *Chem. Rev*., 2010, **110**, 6503–6570.

3 (a) A. Kudo and Y. Miseki, *Chem. Soc. Rev*., 2009, **38**, 253–278. (b) S. R. Lingampalli, U. K. Gautam and C. N. R. Rao, *Energy Environ. Sci.***,** 2013,**6**, 3589-3594.

4 X. Li, J. Yu, J. Low, Y. Fang, J. Xiao and X. Chen, *J. Mater. Chem. A*, 2015, **3**, 2485-2534.

5 X. Qiu, L. Li , J. Zheng, J. Liu, X. Sun and G. Li, *J. Phys. Chem. C*, 2008, **112**, 12242–12248.

6 R. Georgekutty, M. K. Seery and S. C. Pillai, *J. Phys. Chem. C*, 2008, **112**, 13563–13570.

7 H. Qin, W. Li, Y. Xia and T. He, *ACS Appl. Mater. Interfaces*, 2011, **3**, 3152–3156.

8 C. Han, M. Yang, B. Weng and Y. Xu, *Phys. Chem. Chem. Phys.,* 2014, **16**, 16891-16903.

9 Y. Liu, L. Yu, Y. Hu, C. F. Guo, F. M. Zhang and X. W. Lou, *Nanoscale*, 2012, **4**, 183–187.

10 F. Xu, Y. Yuan, H. Han, D. Wu, Z. Gao and K. Jiang *CrystEngComm*, 2012, **14**, 3615-3622.

11 F. Fang, D. X. Zhao, B. H. Li, Z. Z. Zhang, J. Y. Zhang and D. Z. Shen, *Appl. Phys. Lett*., 2008, **93**, 1-3.

12 P. Kundu, P. A. Deshpande, G. Madras and N. Ravishankar, *J. Mater. Chem*., 2011, **21**, 4209-4216.

13 X. Zou, P. Wang, C. Li, J. Zhao, D. Wang, T. Asefa and G. Li, *J. Mater. Chem. A*, 2014, **2**, 4682- 4689.

Physical Chemistry Chemical Physics Accepted Manuscript

14 Y. Tak, H. Kim, D. Lee and K. Yong, *Chem. Commun*., 2008, 4585–4587.

15 J. Jiang, X. Zhang, P. B. Sun and L. Z. Zhang, *J. Phys. Chem. C*, 2011, **115**, 20555–20564.

16 C. Eley, T. Li, F. Liao, S. M. Fairclough, J. M. Smith, G. Smith, S. Chi and E. Tsang, *Angew. Chem. Int. Ed*. 2014, **53**, 7838–7842.

17 Y. G. Lin, Y. K. Hsu, S. Y. Chen, L. C. Chen and K. H. Chen, *J. Mater. Chem.,* 2011, **21**, 324–326.

18 T. Gao, Q. Li, and T. Wang, *Chem. Mater.*, 2005**, 17***,* 887-892.

19 J. Geng, X. D. Jiaac and J. J. Zhu, *CrystEngComm*, 2011, **13**, 193-198.

20 J. Joo, D. Kim, D. J. Yun, H. Jun, S. W. Rhee, J. S. Lee, K. Yong, S. Kim and S. Jeon, *Nanotechnology,* 2010, **21,** 325604-325609.

21 S. Panigrahi and D. Basak, *J. Colloid Interface Sci.,* 2011, **364,** 10–17.

22 Y. Hu, H. Qian, Y. Liu, G. Du, F. Zhang, L. Wang and X. Hu, *CrystEngComm*, 2011, **13**, 3438-3443.

23 S. Cho, J. W. Jang, J. Kim, J. S. Lee, P. W. Choi and K. H. Lee, *Langmuir*, 2011, **27**, 10243–10250**.**

24 S. Martha, K. H. Reddy and K. M. Parida, *J. Mater. Chem. A*, 2014, **2**, 3621-3631.

25 (a) X. Wang, G. Liu, Z. G. Chen, F. Li, L. Z. Wang, G. Q. Lu and H. M. Cheng, *Chem. Commun*., 2009, 3452–3454. (b) X. Wang, G. Liu, G. Q. Lu, H. M. Cheng, *Int. J. Hydrogen Energy, 2010* , **35**, 8199-8205.

26 (a) X. W. Wang, L. C. Yin, G. Liu, L. Z. Wang, R. Saito, G. Q. Lu and H. M. Cheng, *Energy Environ. Sci*., 2011, **4**, 3976–3979. (b) D. Barpuzary, Z. Khan, N. Vinothkumar, M. De,and M. Qureshi, *J. Phys. Chem. C* 2012, **116**, 150–156.

27 X. W. Wang, G. Liu, L. Z. Wang, Z. G. Chen, G. Q. Lu and H. M. Cheng, *Adv. Energy Mater*., 2012, **2**, 42–46.

Physical Chemistry Chemical Physics Accepted Manuscript

28 C. H. Hsu and D. H. Chen, *Nanoscale Research Lett*., 2012, **7;593**, 1-11.

29 G. Yang, W. Yan, Q. Zhang, S. Shen and S. Ding, *Nanoscale*, 2013, **5**, 12432-12439.

30 Z. B. Yu, Y. P. Xie, G. Liu, G. Qing, M. Lu, X. L. Maa and H. M. Chenga, *J. Mater. Chem. A,* 2013, **1**, 2773-2776.

31 (a) J. K. Vaishnav, S. S. Arbuj, S. B. Rane and D. P. Amalnerkar, *RSC Adv*., 2014, **4**, 47637-47642. (b) H. Zhao, Y. Dong, P. Jiang, G. Wang, H. Miao, R. Wu, L. Kong, J. Zhang, C. Zhang, *ACS Sustainable Chem. Eng.*, 2015, **3**, 969-977.

32 P. P. Das, S. Agarkar, S. Mukhopadhyay, M. Unnikrishnan , S. B. Ogale and P. S. Devi, *Inorg. Chem.*, 2014, **53**, 3961-3972.

33 S. Mukhopadhyay, P. P. Das, S. Maity, P. Ghosh and P. S. Devi, *Applied Catalysis B: Environmental,* 2015, **165**, 128–138.

34 L. A. Silva, S. Y. Ryu, J. Choi, W. Choi and M. R. Hoffmann, *J. Phys. Chem. C*, 2008, **112**, 12069–12073.

35 W. Jiang, C. An, J. Liu, S. Wang, L. Zhao, W. Guo and J. Liu, *Dalton Trans.*, 2014, **43**, 300–305.

Physical Chemistry Chemical Physics Accepted Manuscript